Hyperloop Transportation System: Analysis, Design, Control and Implementation

Ahmed S. Abdelrahman, *Student Member, IEEE*, Jawwad Sayeed, and Mohamed Z. Youssef, *Senior Member, IEEE*

Abstract— **This study introduces a novel methodology based on an extensive mathematical analysis, performed from basic electromagnetic principles, with an optimized cost for a magnetic levitation Hyperloop system. This new approach uses both permanent magnets and electromagnets to levitate, propel, and control a pod. The electrodynamic suspension system is emulated as a small pod attached with permanent magnets from the bottom which resembles a short-rotor linear synchronous motor (LSM). A comprehensive finite element analysis using ANSOFT Maxwell software on the effects of the magnetic field distribution of the coils due to the AC current flowing through them is investigated. The effects of the magnetic force exerted on the permanent magnet secondary are examined as well. The whole magnetic levitation system prototype was implemented in the laboratory as a proof of concept in order to validate and verify the simulation results. The simulation results are in full agreement with the mathematical analysis which assure the validity of the design procedure, and the magnetic analysis.**

***Index Terms* — Finite-element analysis (FEA), Hyperloop, linear synchronous motor (LSM), magnetic levitation, magnetic propulsion, permanent magnets, pod design.**

I. Introduction

THERE exists a need for a system that allows everyday commuters the ability to travel from one point to another using a faster, safer, and cheaper mode of transportation. In order to fulfill this need, the Maglev system was developed. The maglev system uses the basic magnetic properties of attraction and repulsion to propel and levitate a pod forwards and backwards at high speed. By using magnetic levitation, the pods avoid the need for wheels, therefore eliminating friction forces from the track. Therefore, pod levitation and propulsion control (PLPC) system continues to extensively progress as a means of futuristic innovative high speed land transportation. There are several different means of levitating and propelling the pod platform centered on the principles of attraction and repulsion of magnets [1]. Not all methods or designs are equally effective.

Manuscript received June 2, 2017; revised September 18, 2017 and October 24, 2017; accepted November 6, 2017.

The authors are with the Department of Electrical, Computer and software Engineering, University of Ontario Institute of Technology (UOIT), Oshawa, Ontario. Canada, (Corresponding author: Mohamed Z. Youssef; phone: 905-721-8668 x5473; fax: 905-721-3370; e-mail: Mohamed.youssef@uoit.ca).

However, each of them has some associated advantages and disadvantages. The first method that is used to achieve magnetic levitation is the electromagnetic suspension (EMS) system [2]. EMS operates solely through attractive forces rather than attractive and repulsive. The train is designed with two C-shaped legs which wrap around a cone shaped track. The attractive force between the underside of the track and the legs overwhelms the force of gravity and thus allow the pod to levitate [3], [4]. Naturally magnets will want to get as close to each other as possible, this results in the complexity of EMS, as to avoid the legs from actually touching the track above a sophisticated control system needs to be put in place to always maintain distance between the train and the track. This allows the train to exhibit levitation even at low speeds. It should be noted that, on either side of the track, there exists additional magnets that assist in the guidance of the train [5], [6]. By having the need to design and implement a more sophisticated control system, the overall cost of implementation goes up. The second method that is utilized to achieve magnetic levitation is the electrodynamic suspension (EDS) systems shown in Fig. 1. This is the technology that is currently used in the Japanese SC Maglev train. Contrary to the EMS system this technology relies on the law of magnetic repulsion as a basis for levitation [7], [8]. The train has superconducting magnets installed in its chassis and guide paths containing metal coils. When current is applied through the guide paths, the train and the guide paths exert a traveling magnetic field. Within the guide path are also passive coils. These passive coils are meant for levitation purposes. As the pod moves over the passive coils, the magnets embedded in the chassis of the pod induce a current onto the passive coils. Subsequently, the train is able to levitate and propel because of the repulsive and attractive forces of the north and south poles. Because the system requires induced current to power the passive coils for levitation, the pod will only levitate when the force of the magnetic field produced by the passive coils equals the gravitational force of the pod. Thus this system is self- controlling and therefore there is no need for an additional sophisticated control system. However since the passive coils require induced current, the pod must already be moving at a certain speed before the forces can cancel out, due to this the pod is EDS systems are equipped with wheels that are required for slow speeds before levitation can take place [2], [9].

This study set out to investigate an alternative method of applying the EDS system. Traditionally EDS systems take advantage of passive levitation coils, where a moving magnetic

field induces a current on the passive coils which then produces a magnetic field. The traditional EDS system can be modelled as a LSM for the propulsion system, and a linear induction motor (LIM) for the levitation system and peak force control [10], [11]. Conceptually, a linear motor is a rotary motor where its rotor and windings have been cut open and laid out flat. The purpose of this paper is to substitute the LIM of the levitation system with a LSM, so that both the propulsion system and levitation system utilize a LSM. The reason for this change is to establish levitation at standstill and at low speeds, thus eliminating the need for wheels attached to the pod. For the prototyping purposes the LSM is implemented using windings going across the track which are powered using AC power, the track is modeled as a long stator, and the pod as a permanent magnet short rotor as shown in Fig. 2. The pod acts like a short rotor where the permanent magnets are the equivalent of a DC power supply in series with a winding.

II. DESIGN AND ANALYSIS

a. Machine Layout

In order to test the theory and simulations, practically, a test bench is developed. The test bench is a short piece of track modeled similar to the stator of a LSM and a pod that is similar to the rotor of a LSM. The track consists of solenoids going along the side and along the bottom of the track to resemble the windings of a long stator, whereas the pod has six permanent magnets embedded at the bottom and two embedded on each side to interact with the windings. The pod resembles a short rotor for the LSM. The long stator of the LSM requires AC power to flow through the windings to create electromagnets with alternating polarity, and the permanent magnets embedded in the pod are the equivalent of a dc excitation winding [8], [12]. Interaction between the magnetic field and armature currents produces the thrust force. The speed of traveling magnetic wave depends on the power supply's frequency [9], [13].

In order to calculate the correct specifications for the LSM test bench, some values need to be considered as constants. In order to calculate the correct number of turns per winding, the magnetic field of the permanent magnets at distance z is evaluated [8], [14]. Equation (1) can be used to calculate the magnetic flux density assuming the use of a cube shaped permanent magnet:

$$B = \frac{B_r}{\pi}\left[\tan^{-1}\left(\frac{LW}{2z\sqrt{4z^2+L^2+W^2}}\right)\tan^{-1}\left(\frac{LW}{2(H+z)\sqrt{4(H+z)^2+L^2+W^2}}\right)\right] \quad (1)$$

In order to achieve levitation, the repulsive force between the permanent magnet and the coil underneath it must be equivalent to the force of gravity. The force of a solenoid at a distance z can be described by the following equations:

$$F_s = \frac{N^2 I^2 \mu_0 A}{2z^2} \quad (2)$$

$$A = \pi r^2 \quad (3)$$

Based on Fig. 3, it can be deduced that in order to achieve levitation;

$$F_{PM} = F_{Gravity} \quad (4)$$

b. Pod Design

The short rotor for the LSM will be designed as a pod. The pod will have permanent magnets embedded within it. There are six permanent magnets at the bottom of the pod that interact with the levitation solenoids at the bottom, and there are two permanent magnets on each side of the pod that interact with the propulsion solenoids lined along the side of the track. The short rotor design is shown in Fig. 5 as the CAD drawing.

In order to achieve levitation and propulsion it was important to understand the mass of the object that needs to be moved. Since the pod design was 9 by 5 by 3 inches, and because the pod was hollow, the thickness of each steel plate is predetermined. Therefore, all that had to be calculated was the mass and surface area. The thickness of the steel was known to be 0.125 inch. The mass per square inch of steel was known to be 0.035 pound/inch^2. Surface 1 of the pod is illustrated in Fig. 4.

The area of surface 1 of the pod was calculated as follows:

$$A_{s1} = (length)(width) = 12.7 * 7.62 = 96.77 \text{ cm}^2$$

The mass of surface 1 of the pod is given by the following:

$$m_{s1} = 15.9 * 15 = 238.5\ g$$

The same calculations were done for both surface 2 and surface 3 as follows:

$$A_{s2} = 22.86 * 7.62 = 174.19 \text{ cm}^2$$

$$m_{s2} = 15.9 * 27 = 429.3\ g$$

$$A_{s3} = 22.86 * 12.7 = 290.32 \text{ cm}^2$$

$$m_{s3} = 15.9 * 45 = 715.5\ g$$

The total mass of the metal pod alone is:

$$m_{metal} = (238.5 + 429.3 + 715.5\ )(2) = 2766.6\ g$$

The design required 32 magnets to be utilized on the pod.

$m_{magnet} = 14\ g$, then $m_{magnets} = (14)(32) = 448$ g.

In order to power the control instrumentation, a battery was situated on the pod. The mass of the battery with the control instrumentation is given below:

$m_{control} = 208\ g$

Therefore, the total mass of the pod is:

$m_{total} = 3422.6\ g$

Since the mass of the pod is now known, the gravitational force that needs to be countered was calculated.

$\vec{a}_{gravity} = 9.8\ m/s^2\ \ [down]$

$\vec{F}_{pod} = ma = 3.42 * 9.8 = 33.5\ N\ [down]$

This article has been accepted for publication in a future issue of this journal, but has not been fully edited. Content may change prior to final publication. Citation information: DOI 10.1109/TIE.2017.2777412, IEEE Transactions on Industrial Electronics

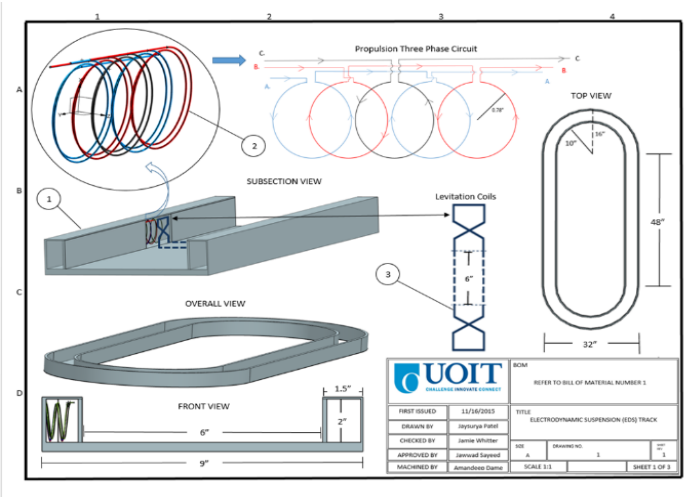

Fig. 1. Electrodynamic Suspension system

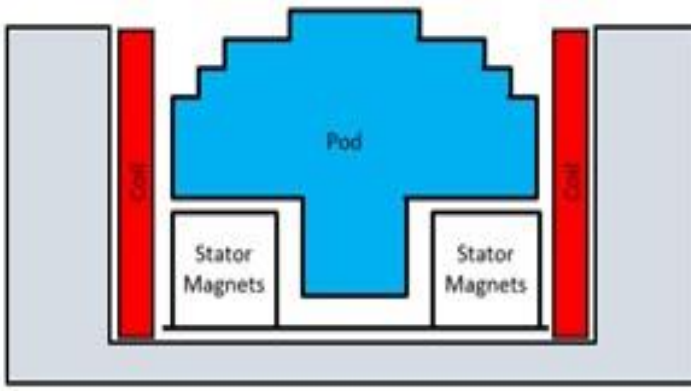

Fig. 2. Short rotor LSM

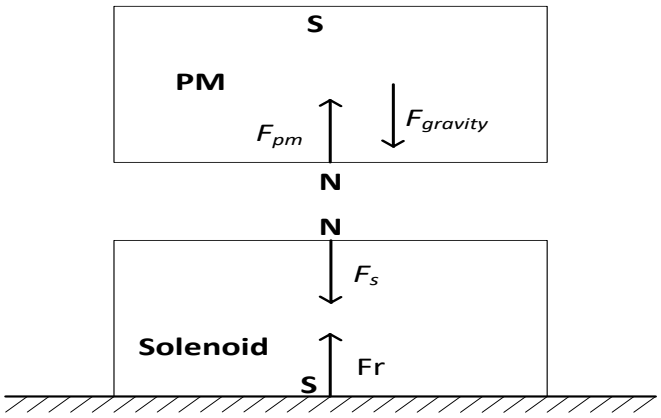

Fig. 3. Free body diagram of single permanent magnet and solenoid

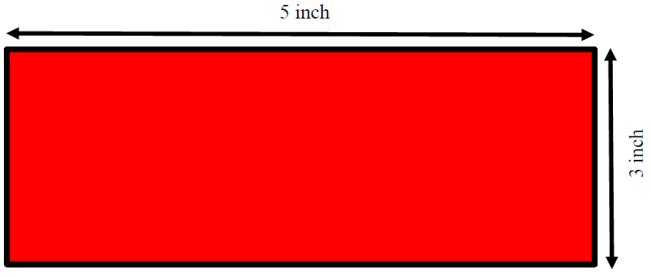

Fig. 4. Surface 1 of the pod

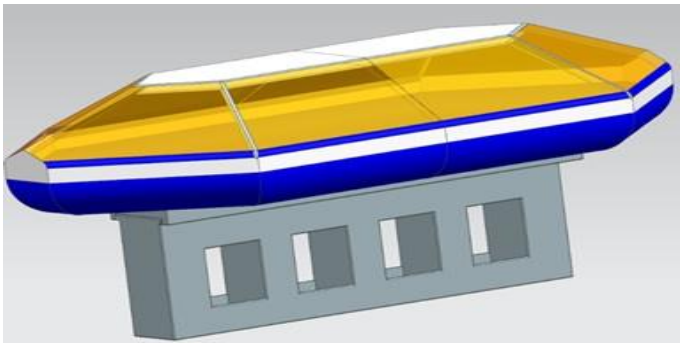

Fig. 5. CAD drawing for pod

c. *Halbach array calculations*

The Halbach array is a special arrangement of magnets that reinforce the magnetic field on one side while greatly reducing the magnetic field on the other side to almost zero [6], [7], [12]. The Halbach array comes in different arrangement lengths. For the PLPC design an eight magnet arrangement is utilized. Fig. 5 is a single unique arrangement of the Halbach array that is utilized in this design.

Magnetic field strength at the surface of the Halbach array was calculated using the following equation:

$$B_o = B_r\left(1 - e^{-2\pi d/\lambda}\right)\left[\frac{\sin\left(\frac{\pi}{Nm}\right)}{\frac{\pi}{Nm}}\right] \tag{5}$$

$$B_o = 1.48\left(1 - e^{\frac{-(2)(\pi)(0.0127)}{(0.1016)}}\right)\left(\frac{\sin\left(\frac{\pi}{8}\right)}{\frac{\pi}{8}}\right) = 0.7847\ T \tag{6}$$

The Halbach array produces a sinusoidal magnetic field. As a result the x and z components of the magnetic field produced by the Halbach array are modeled by the following set of equations.

$$\mathrm{B_x} = \mathrm{B_o}\sin\left(\frac{2\pi}{\lambda}\mathrm{t}\right) \tag{7}$$

$$\mathrm{B_z} = \mathrm{B_o}\cos\left(\frac{2\pi}{\lambda}\mathrm{t}\right) \tag{8}$$

$$B_x = 0.7847\,sin(61.8t) \tag{9}$$

$$B_z = 0.7847\,cos(61.8t) \tag{10}$$

If the Halbach array moves at velocity, it creates a magnetic field frequency of which is modeled below by the following equation:

$$\omega = \frac{2\pi v}{\lambda}\ \frac{rad}{sec} \tag{11}$$

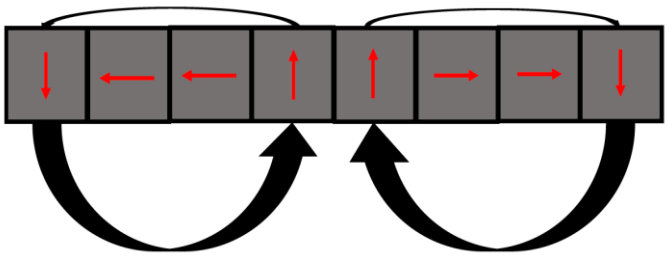

Fig. 6. Halbach array calculations

d. Track design

In a LSM, the rotor requires an active stator to interact with in our case, the stator will be the track itself. The levitation coils at the bottom of the track will act as a stator and the propulsion coils lined along the sides of the track will represent the second stator [15], [16].

The base of the prototype track is constructed using a 49.53 cm long by 15.24 cm wide by 1.91 cm thick pine wood plank. The sides of the track are two 49.53 cm long by 13.97 cm high by 1.27 cm thick wood planks that are fastened to the outside of the base of the track with a total of eight flat socket head 6*1.25 inch screws. The prototype track also possesses two end walls. The dimensions of the end walls are 17.78 cm long by 13.97 cm high by 1.91 cm thick. The end walls are fastened to the base of the track and the side walls with a total of five 6*1.25 inch screws.

The first pair of levitation coils shown in Fig. 6 are placed 3.81 cm away from the end walls and 3.18 cm away from the side walls. A thick spacer 49.53 cm long, 3.18 cm wide, and 1.91 cm is placed in between the outside of the levitation coils and the outer wall. This ensures minimal lateral displacement of the coils. Twelve more pairs are continued along the base of the track, where each levitation coil in a pair is separated by a 1 cm thick shim. Small holes are drilled in the bottom of the base of the track, where at the center of each coil. This allows the leads of the coils to come through the track, giving it a cleaner appearance.

The propulsion coils for the PLPC project also shown in Fig. 7 are placed on the track's side walls. The propulsion coils rest on a wooden platform that sits on three dowels that are evenly spaced through each side wall. Again, the leads from the propulsion coils are fed through small holes that are created in the center of each coil, giving the track a cleaner appearance. The first propulsion coil on each side of the track begins 5.72 cm from the end wall, and continues side by side through the remainder of the track. The top of the propulsion coils is 8.89 cm from the base of the track's platform.

e. Control System

The assembly of the control system involves several facets. These include the assembly of the inverter circuit, the FPGA board, and the on pod microcontroller. When transferring the control system components from destination to destination, the assembled inverter circuit with the attached FPGA board, and microcontroller are carefully handled. The circuits are placed in individual boxes with protection to prevent the breaking of any connections. The components of the control system include: a breadboard, jumper cables, resistors, inductors, capacitors, MOSFETs, FPGA board, Bluetooth module, infrared sensors, microcontroller, and an IMU. The original design for the controller called for the use of a microcontroller over an FPGA board and a microprocessor. As the PLPC system progressed and its complexity was realized, it was determined that the controller should be the option with the greatest processing power. Hence, the FPGA board was chosen over the microcontroller.

A snubber circuit was added in parallel with each MOSFET to reduce the stress on the transistors. The snubber circuits contain a capacitance of 10 μF and a resistance of 1000 Ω. It should be noted that two pull down resistors and two pull up resistors of 1000 Ω were used. The complete schematic diagram of the control system can be shown in Fig. 8. The feedback block utilizes the data from the onboard sensors, gyroscope and accelerometer sent via Bluetooth from the pod to the FPGA board. Once the FPGA board has the data, it then sends the data into the Kalman filter which then makes an estimation as to the position of the pod and then corrects it by sending a corrective feedback signal. The FPGA board then utilizes this signal to either increase or decrease the current of the coils. Utilizing the on board sensor data will be effective for correcting destabilization due to external disturbances, such as a seismic event.

One of the crucial parts of the control system is the inverter control. The inverter circuit is controlled via pulse width modulation (PWM) signals. The way this is done is by feeding inverted PWM signals into diagonal MOSFETs, thus causing current to flow in both directions of the load. Typically, there are two common PWM signals used. The first type of PWM signal is a digital PWM, which is just a periodic signal that goes high for some percentage of its period and then low for the remainder. The second is a sinusoidal PWM signal which compares a sinusoidal wave with a triangle wave and forms a PWM signal that has multiple duty cycles within one period. For simple applications, a digital PWM would suffice. However, in this application using a digital PWM would create many harmonics and would cause multiple issues due to back EMF. For this paper a digitally conceived sinusoidal PWM signal is required.

The PWM was implemented using a microcontroller by utilizing a look up table that contained the sine values. By comparing the look up table values with a down counter a sinusoidal PWM was achieved. By using these techniques, we were able to output a digital sinusoidal wave, and a digital triangle wave, Fig. 8.

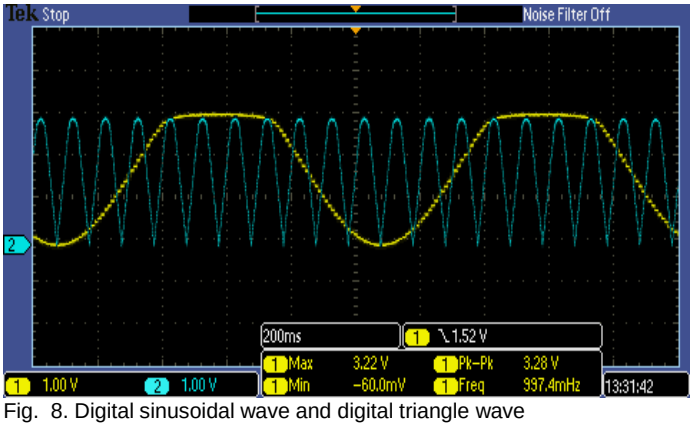

Fig. 8. Digital sinusoidal wave and digital triangle wave

The two digital signals were then fed through a digital comparator to form the sinusoidal PWM, zoomed in snapshot of the PWM signal is in Fig. 9.

The most significant part of the control system is the Kalman Filter. The Kalman filter is a filter that is used to predict the next state of the system. The state we will want to predict is the position of the pod with respect to the levitation coils. The idea is to have the pod always be parallel to the levitation coils so that we can avoid tilting and tipping in the system.

This article has been accepted for publication in a future issue of this journal, but has not been fully edited. Content may change prior to final publication. Citation information: DOI 10.1109/TIE.2017.2777412, IEEE Transactions on Industrial Electronics

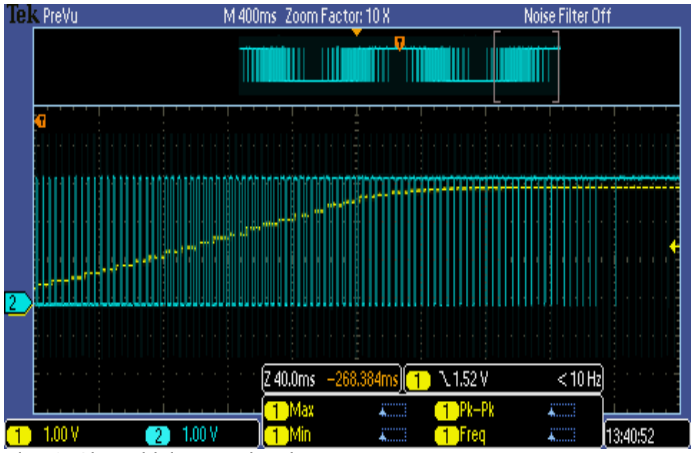

Fig. 9. Sinusoidal PWM signal

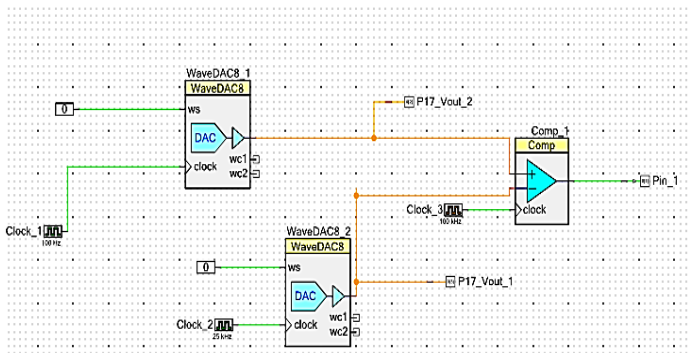

Fig. 10. Sinusoidal PWM signal schematic

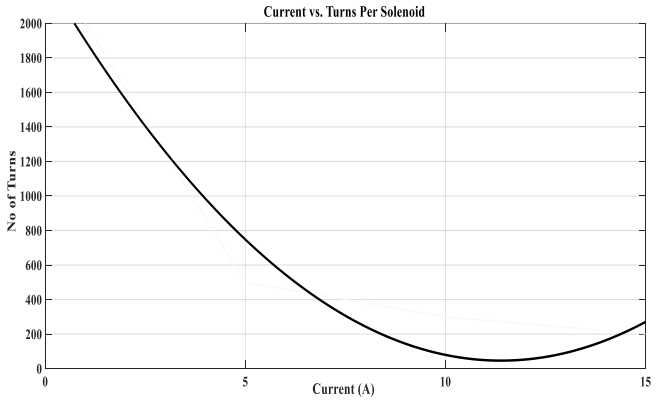

Fig. 11. Number of turns versus current to produce the necessary solenoid force

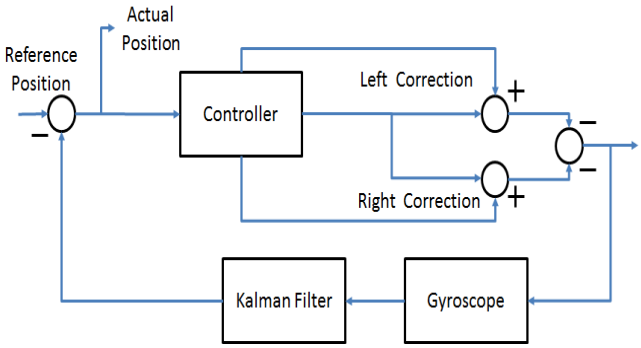

Fig. 12. Schematic diagram of the proposed control system

The Kalman filter has two sets of equations. The first set of equations is known as the prediction equations as listed below:

$$X = Ax_{k-1} + Bu_{k-1} \tag{13}$$

$$p = APA^T + Q \tag{14}$$

The second set of equations is known as the update equations. The update equations are listed below:

$$K = pH^T(HpH^T + R)^{-1} \tag{15}$$

$$x_k = X + K(z - HX) \tag{16}$$

$$Px_k = (I - KH)_p \tag{17}$$

According to the design parameters, the equivalent second order equation of the overall system was calculated to have a damping factor of 0.65 and overall gain of 0.45. This guarantees that the overall system is made to be underdamped in nature. With the above parameters, a healthy maximum overshoot of 10% has been attained. This was achieved in accordance with the industry standard for the transportation industry. The railway propulsion standard of rolling stuck in the transportation has to follow the EN 50155 standard regulations. That being said, the overall control system has to guarantee that the system is underdamped with a reasonable overshoot percentage and settling time so the overall settling time of the system was 80% of the overall system. Based on the above system, the design was made carefully to follow this industry standard.

f. Prototype Design

To design a successful prototype, all the design constraints should be taken into consideration. For this particular analysis the major constraint is the need for an AC power supply; the AC power supply is essential to the design, due to the fact that propulsion is not possible with DC power, and because DC power is inherently unstable [16], [17]. To get around the lack of AC power supply, a DC to AC inverter circuit had to be designed. With the DC power supply, our current is limited to 15 A, thereby restricting our AC current running through the windings to 15 A as well. The radius of the solenoid is held constant at 1 cm. The permanent magnets have a length, width, and height of 1.27 cm, and from the datasheet it is known that the repulsive force at 1.27 cm away from the surface of the permanent magnet is 6.27 N. Since the short rotor weighs 0.68 kg, the force of gravity is as follows:

$$F_{Gravity} = mg \tag{12}$$

Substituting by the weight of the short rotor and acceleration due to gravity into (5), we obtain:

$$\vec{F}_{Gravity} = 6.66\ N\ downwards$$

Since there are always six solenoids under the short rotor, the force of gravity acting on the short rotor can be split into six

portions. Therefore, the force which the solenoid must produce using equation (2) is as follows:

$$\vec{F}_s = 7.38\ N\ upwards$$

Now that all the constraints have been specified, the optimal number of turns can be calculated using equation (2) by varying the current:
As can be seen from Fig. 7, the optimal number of turns is 310 as this only requires 8 A of current to be pushed through the windings.

1. *Pod Implementation*

After developing the designs for the short rotor, the next step in the process was to implement the design. This is achieved by having the pod 3D printed, to reduce weight, and then embedding the permanent magnets within it. The pod overall implementation is shown in Fig. 13. All the materials used to construct the pod were made of non-magnetic elements so that there should be no interference with the solenoid and permanent magnet interaction.

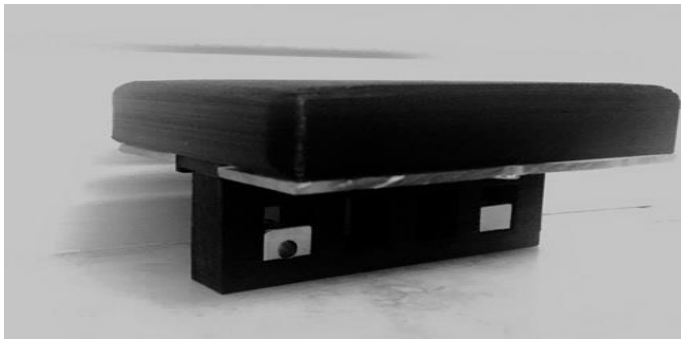

Fig. 13. 3D printed pod

2. *Track Implementation*

In order to implement the track, we used wood to make the base, and we used magnet wire to form the solenoids. The implemented track is as follows:
Fig. 14 shows the final track implementation that is used for the test bench. We will be using pre-manufactured wireless power transfer coils. These will supply us with the required magnetic flux for the propulsion system. Since wireless power transfer coils are significantly smaller than the hand wound copper coils, we were also able to reduce costs on the propulsion system by $50. The design of our track also had to account for the switch to the wireless power transfer due to space limitations. The changes allowed us to reduce the width of the track by 4cm.

III. SIMULATION RESULTS

a. *Inverter Simulation*

The next stage in ensuring a working prototype is to simulate the results that are obtained through the design analysis, and then fine tuning those simulations until the desired result is obtained. The first step is to simulate and design an optimal inverter circuit as shown in Fig. 15.

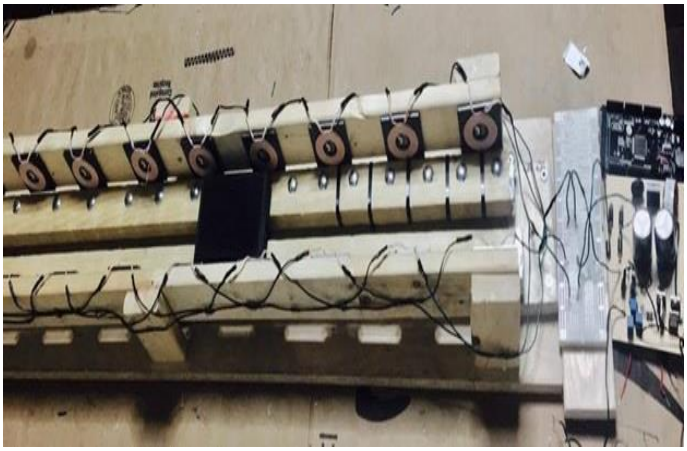

Fig. 14. Track implementation

Without an inverter circuit, producing a clean AC sinusoidal waveform accompanied by the highest amount of current possible, the solenoids will not be able to produce the required thrust force, and accordingly cannot generate the highest possible force to achieve levitation.

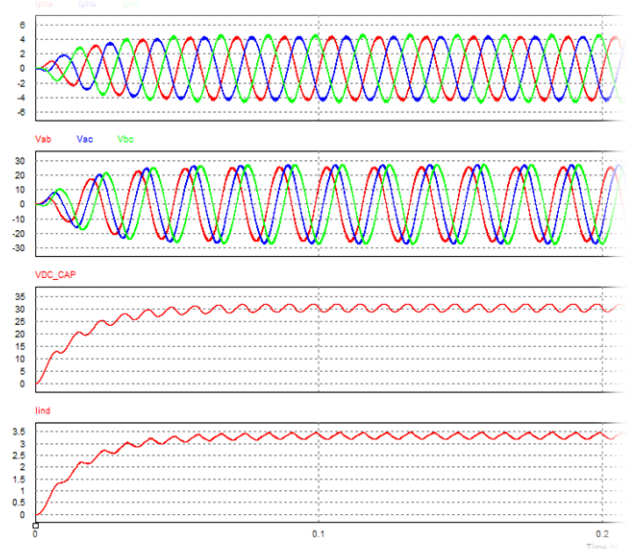

Fig. 15. Simulation results of output current, voltage, inductor current and capacitor voltage

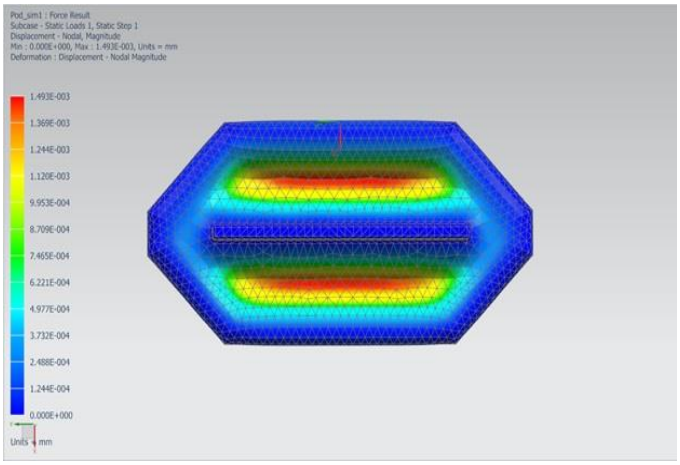

Fig. 16. Forces on the POD using FEA: Top view

This article has been accepted for publication in a future issue of this journal, but has not been fully edited. Content may change prior to final publication. Citation information: DOI 10.1109/TIE.2017.2777412, IEEE Transactions on Industrial Electronics

b. Solenoid Simulation

The next stage in the simulation process is to simulate the magnetic field strength caused by the active coils once the inverter circuit supplies power to them as can be seen in Fig. 17.

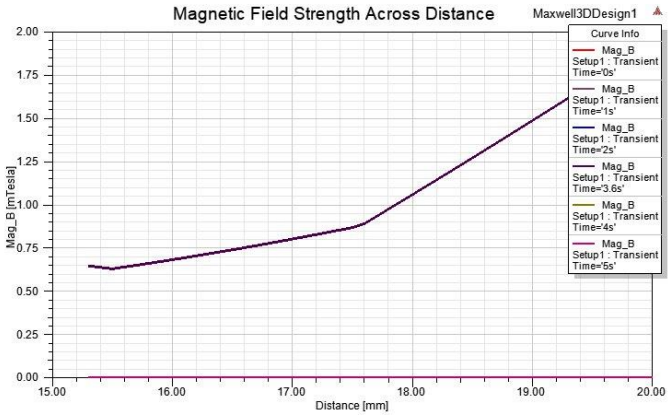

Fig. 17. Simulated magnetic field in the Z direction due to solenoid

It is noticed that the direction of the magnetic field changes from solenoid to solenoid. The reasoning for this is because the signal continually alternates [18], [19]. Depending on the frequency of the current coming from the supply the magnetic poles alternate at that rate. It is also noted that there is an abundance of flux leakage as the coils are air cored, which causes the magnetic field to be less concentrated, and overall reduces the produced force. In Fig. 18, the magnetic field in the Z direction is observed to be 0.026 Tesla.

As seen in Fig. 19, it can be noted that the force produced by an air core, 310 turns solenoid only produces 90 mN of force.

Due to the fact that flux leakage was not taken into account while performing the design analysis, the simulation results vary greatly from the design analysis. In order to obtain results that are acceptable for the purposes of this analysis, fine tuning of the design parameters was needed.

The first design change that is implemented is concentrating the magnetic flux so that the flux lines do not escape. In order to accomplish this, a soft iron core is added to the simulation. By so doing, the relative permeability is increased greatly, thus allows less flux leakage. The next design change is to alter the number of turns to a reasonable amount, in this case the number of turns are altered to 430 turns. Finally, the current that is supplied to the solenoids is at its maximum of 15A. After having made all these design alterations, the following results were obtained.

From Fig. 20, it is observed that the magnetic field has now been amplified to 6.7 Tesla, and the flux lines are all contained within the soft iron core as there are none visibly escaping.

Observing Fig. 21 obtained through simulation, it can be deduced that the magnetic force produced by the solenoid in the Z direction is 7.85 N.

IV. EXPERIMENTAL RESULTS

The inverter circuit includes many stages of testing. The construction of the inverter circuit was successful and the snubber circuits minimized the heat through the MOSFETs. It is evident that the force produced by the coils is as expected. The graph above illustrates a maximum force of only 20 Newtons per coil. Therefore, both the simulation was performed correctly and the coils produce the force that was expected based on calculations. The above Figures illustrate the output of the inverter circuit. Improvements are achieved by adding a filter to the circuit. The filter creates an alternating sinusoidal current with reduced harmonics.

The final output of the inverter circuit was to depict a clean sinusoidal wave as can be seen in Fig. 22 to Fig. 25.

Fig. 18. Simulated magnetic force produced by solenoid in the Z direction at 0.5 inch

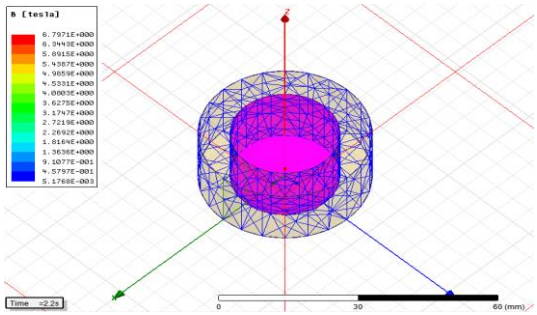

Fig. 19. Altered simulation of AC solenoid

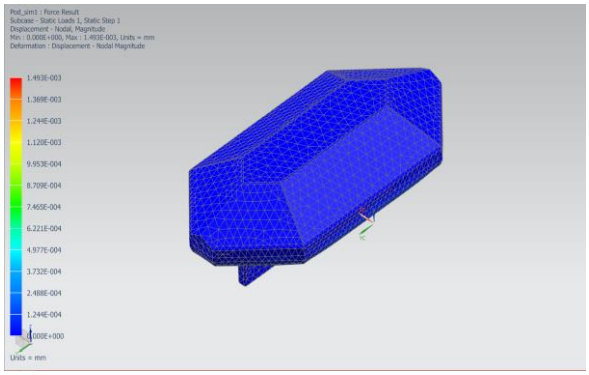

Fig. 20. Minimal vertical forces on the Pod: Control feedback effect

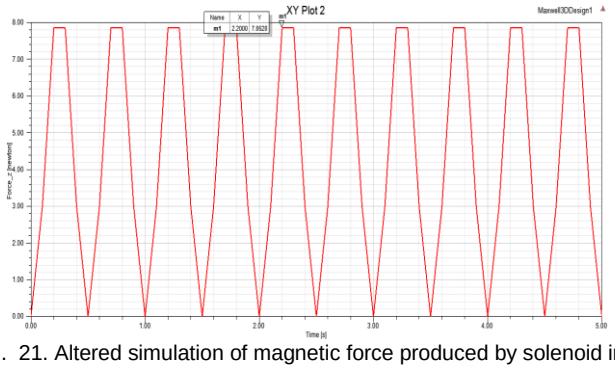

Fig. 21. Altered simulation of magnetic force produced by solenoid in the Z direction at 0.5 inch

This article has been accepted for publication in a future issue of this journal, but has not been fully edited. Content may change prior to final publication. Citation information: DOI 10.1109/TIE.2017.2777412, IEEE Transactions on Industrial Electronics

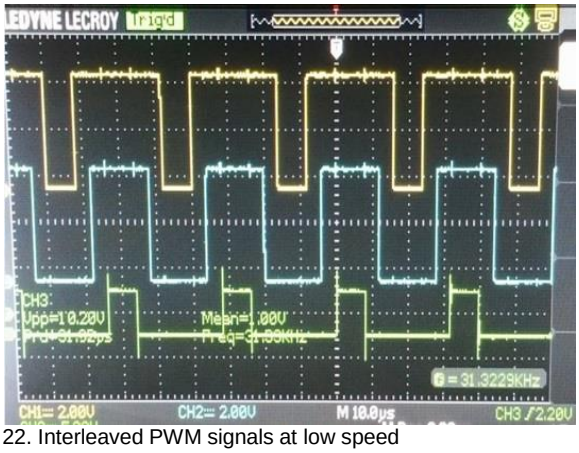

Fig. 22. Interleaved PWM signals at low speed

Fig. 23. Inverter PWM signals at high speed; middle stream is for one leg

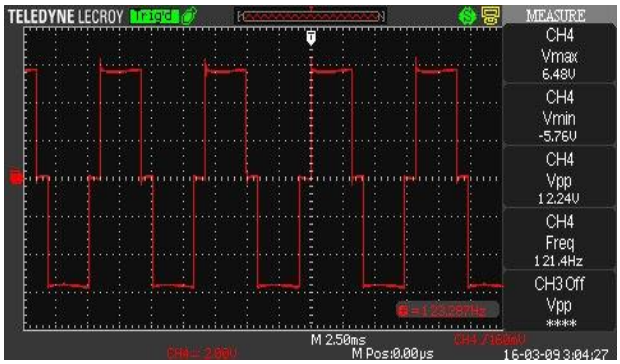

Fig. 24. Output AC signal with resonance filter

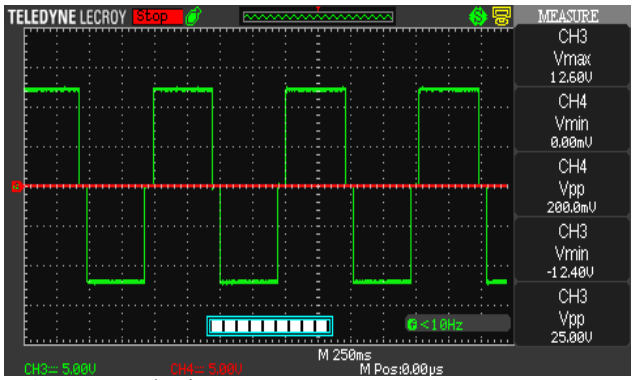

Fig. 25. Inverter circuit output

V. CONCLUSION

The design and prototyping analysis of a PLPC system is presented in this paper. Based on a detailed analytical approach, the design is analyzed and the design parameters are set. After the design constraints and parameters are determined, a finite element simulation using ANSYS Maxwell was used to verify the analytical approach, and to determine the appropriate design specifications of the PLPC, thus confirming the validity of the design. The end product illustrates an innovative approach to EDS technology to produce a functional product.

APPENDIX

TABLE A.1
MATERIALS USED IN EDS TRACK

ELECTRODYNAMIC SUSPENSION (EDS) TRACK BILL OF MATERIAL 1				
Item	Qty.	Manufacturer	Description	Part Number
1	1	N/A	Wooden track assembly, 21"x 10.25" x 5.375"	N/A
2	1700 ft	Amazon Export Sales LLC	Propulsion coils, 22 AWG magnet wire	UEV22
3	1700 ft	Amazon Export Sales LLC	Levitation coils, 22 AWG magnet wire	UEV22

TABLE A.2
MATERIALS USED IN POD DESIGN

POD Design Bill of Material 2				
Item	Qty.	Manufacturer	Description	Part Number
1	1	N/A	Plastic pod assembly, 5" x 2.75" x 1.75"	N/A
2	10	Magcraft	Super strong magnets, neodymium-iron-boron rare earth magnets	MW18

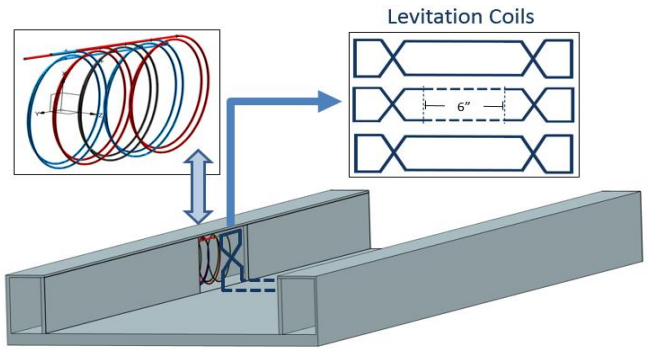

Fig. 26. Track Design

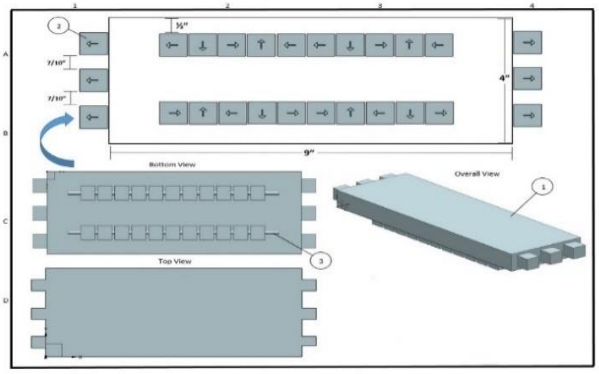

Fig. 27. Pod Design

REFERENCES

[1] M. A. M. Cheema, J. E. Fletcher, D. Xiao, and M. F. Rahman, "A Direct Thrust Control Scheme for Linear Permanent Magnet Synchronous Motor Based on Online Duty Ratio Control," *IEEE Trans. Power Electron.*, vol. 31, no. 6, pp. 4416–4428, 2016.

[2] Z. Long, G. He, and S. Xue, "Study of EDS & EMS hybrid suspension system with permanent-magnet halbach array," *IEEE Trans. Magn.*, vol. 47, no. 12, pp. 4717–4724, 2011.

[3] H. W. Lee, K. C. Kim, and J. Lee, "Review of Maglev train technologies," *IEEE Trans. Magn.*, vol. 42, no. 7, pp. 1917–1925, 2006.

[4] L. Songqi, Z. Kunlun, L. Guoqing, and G. Wei, "EMS maglev vehicles model reference adaptive control," *Chinese Control Conf. CCC*, vol. 2015–Septe, pp. 2989–2993, 2015.

[5] H. W. Lee, C. B. Park, and J. Lee, "Improvement of thrust force properties of linear synchronous motor for an ultra-high-speed tube train," *IEEE Trans. Magn.*, vol. 47, no. 11, pp. 4629–4634, 2011.

[6] Q. HAN, "Analysis and Modeling of the Eds Maglev System Based on the Halbach Permanent Magnet Array," 2004.

[7] R. F. Post and D. D. Ryutov, "Inductrack: A simpler approach to magnetic levitation," *IEEE Trans. Appl. Supercond.*, vol. 10, no. 1, pp. 901–904, 2000.

[8] K. Chen, Y. Sun, and B. Liu, "Interior permanent magnet synchronous motor linear field-weakening control," *IEEE Trans. Energy Convers.*, vol. 31, no. 1, pp. 159–164, 2016.

[9] W. Zhao, M. Cheng, J. Ji, R. Cao, Y. Du, and F. Li, "Design and analysis of a new fault-tolerant linear permanent-magnet motor for maglev transportation applications," *IEEE Trans. Appl. Supercond.*, vol. 22, no. 3, pp. 0–3, 2012.

[10] T. A. Faculty, N. Chayopitak, and I. P. Fulfillment, "Performance Assessment and Design Optimization of Linear Synchronous Motors for Manufacturing Applications Performance Assessment and Design Optimization of Linear Synchronous Motors," *Mech. Eng.*, no. August, 2007.

[11] L. Cailin and W. Dongmei, "The Permanent Magnet Synchronous Linear Motor Position Control Based on Fuzzy Neural Network," *2013 5th Int. Conf. Intell. Netw. Collab. Syst.*, no. 12, pp. 602–606, 2013.

[12] Z. Zhang, L. Shi, Q. Ge, and Y. Li, "Characteristics analysis of single-sided ironless linear synchronous motor based on permanent magnet Halbach array," *2015 18th Int. Conf. Electr. Mach. Syst. ICEMS 2015*, pp. 275–278, 2016.

[13] B. Kou, L. Zhang, Y. Zhang, and Y. Jin, "Modeling and Design of Testing Platform for Permanent Magnet Linear Synchronous Motor," no. c, pp. 1535–1538, 2014.

[14] D. Cui, R. Wei, J. Liu, and Q. Ge, "Linear synchronous motor drive system based on proportion resonant current controller in maglev transportation," *2014 17th Int. Conf. Electr. Mach. Syst. ICEMS 2014*, pp. 1289–1292, 2015.

[15] U. Hasirci, A. Balikci, Z. Zabar, and L. Birenbaum, "A novel magnetic-levitation system: Design, implementation, and nonlinear control," *IEEE Trans. Plasma Sci.*, vol. 39, no. 1 PART 1, pp. 492–497, 2011.

[16] U. Hasirci, A. Balikci, Z. Zabar, and L. Birenbaum, "Experimental Performance Investigation of a Novel Magnetic Levitation System," *IEEE Trans. Plasma Sci.*, vol. 41, no. 5, pp. 1174–1181, 2013.

[17] J.-S. Shin, R. Watanabe, T. Koseki, H.-J. Kim, and Y. Takada, "The Design for Cogging Force Reduction of a Double-Sided Transverse Flux Permanent Magnet Linear Synchronous Motor," *IEEE Trans. Magn.*, vol. 50, no. 11, pp. 1–4, 2014.

[18] M. A. M. Cheema, J. E. Fletcher, D. Xiao, and M. F. Rahman, "A Linear Quadratic Regulator Based Optimal Direct Thrust Control of Linear Permanent Magnet Synchronous Motor," *Ind. Electron. IEEE Trans.*, vol. PP, no. 99, p. 1, 2016.

[19] J.-F. Lieu, C.-S. Ting, B.-W. Shi, and Y.-N. Chang, "Adaptive backstepping control for permanent magnet linear synchronous motor servo drive," *IET Electr. Power Appl.*, vol. 9, no. 3, pp. 265–279, 2015.

Ahmed S. Abdelrahman (S'16) received the B.Sc. degree in electrical engineering with distinction from the Faculty of Engineering, Cairo University, Cairo, Egypt, in 2010, and the M.Sc. degree (Hons.) in electrical engineering from the Faculty of Engineering, Cairo University, Cairo, Egypt, in 2013. He is currently working toward the Ph.D. degree in electrical engineering from the University of Ontario Institute of Technology (UOIT), Oshawa, Canada. He is the team leader of Power Electronics and Drives Applications Lab (PEDAL) and part of the SpaceX team at UOIT. His research interests include automotive applications, electric vehicles, electromagnetic design for new transportation systems and control of power electronics.

Jawwad Sayeed received a B. Eng degree in electrical engineering from the University of Ontario Institute of Technology, Canada in 2016. He is currently pursuing a M. ASc. degree in electrical engineering at the University of Ontario Institute of Technology, Canada. He is a member of Power Electronics and Drives Applications Lab (PEDAL) and part of the SpaceX team at UOIT. Also, he is a junior hardware design engineer at Emphatec. His research area mainly includes power electronics.

Mohamed Z. Youssef (SMIEEE); completed his Ph.D. in Power Electronics at the ePEARL Lab, Queen's University, Canada in 2005, where he was later an adjunct Assistant Professor involved in teaching and research. In 2007, he joined Bombardier Transportation where he worked as a Senior Research and Development engineer. In 2012, he joined Alstom Transport as a Research and Development Engineering Manager. His research interests include Electromechanical Systems for the Transportation Industry, Electromagnetic Compatibility (EMC) for the Railways and Power Electronics Applications for the Information Technology. Mohamed was the motor and electronics manager for Armstrong Pumps before coming back to Academia. Dr. Youssef is currently an Assistant Professor in the ECSE department at the University of Ontario, Institute of Technology (UOIT) in Canada. He is the director of power electronics and drives lab (PEDAL) at UOIT and the university leader of Space-X team. He has more than 80 papers in the top tier IEEE journals and conferences with 5 US/Canadian patents. He is a fellow of the Canadian Council of Professional Engineers. He is a senior IEEE member and a professional engineer in the province of Ontario. He is an appointed Adjunct Professor at the Royal Military College (RMC) of Canada. Mohamed is a member of the IEEE committee of Transportation standards and a fellow expert of the Canadian government on many future infrastructure directives. He was recently appointed to the consultancy board of Sustainable Development Technology Canada (SDTC); He is also a member of the Egyptian syndicate of Engineering.